The organic stratigraphy of Ontong Java Plateau Tuff correlated with the depth related presence and absence of putative microbial alteration structures

Graham Purvis[1*], Cees van der Land[1] Naoko Sano[2], Charles Cockell[3], Anders Barlow[4], Peter Cumpson[2], Elisa Lopez-Capel[1] and Neil Gray[1]

[1]Geosciences, School of Natural and Environmental Sciences, Devonshire Building, Newcastle University, Newcastle-upon-Tyne, NE1 7RU

[2]National ESCA and XPS Users' Service (NEXUS), Stephenson Building, Newcastle University, Newcastle-upon-Tyne, NE1 7RU

[3]UK Centre for Astrobiology, School of Physics and Astronomy, James Clerk Maxwell Building, the King's Buildings, University of Edinburgh.

[4]Centre for Materials and Surface Science, Department of Chemistry and Physics, La Trobe University, Melbourne, Victoria 3086, Australia

*Corresponding author: g.w.h.purvis@ncl.ac.uk

Running title: Organic stratigraphy of Ontong Java Plateau Tuff

Key words

Stratigraphy

Ontong Java Plateau

Organics

Basaltic glass

Microtubules

Tuff

Abstract

Structures in geological samples are often interpreted as fossilised life, however, such interpretations are equivocal, as abiotic processes can be invoked to explain their presence. Thus, additional lines of chemical evidence are invaluable in confirming or refuting such morphological evidence. Glass shards in tuff from the Ontong Java Plateau (OJP) contain microtubular structures that are in close proximity to functionalised nitrogen substituted aromatic compounds, that may be indicative of the chemical remnants of biological activity. The organic composition of the OJP tuff containing microtubular alteration structures, was compared with tuff without such features. In addition, organic matter associated with horizons with compacted remnants of woody material buried in the OJP tuff and overlying pelagic calcareous foraminifer sediment were also characterised, to ascertain the provenance of the organic matter found in the OJP tuff. As a further control, the organic material in sub-marine and terrestrial basalts from other locations were also characterised providing further evidence to support the view that the organic matter in the OJP tuff is authigenic. Carbon-nitrogen chemistry was detected across all OJP tuff samples irrespective of the presence or absence of microtubular features, but were not detected in either the wood material, the overlying pelagic sediments or in the basalts from other locations. The results indicate no direct link between the OJP nitrogenous organic compounds and the presence or absence of microtubular features.

1.0 Introduction

The alteration of rock texture and composition occurs through many physical and chemical processes which can also have a biological component. One such process is the formation of distinctive micron-sized cavities, which are putatively made by microorganisms, and have been interpreted as a visible indicator of the fossilised traces of microbial activity (Fisk *et al.*, 1998; Alt and Mata, 2000; Staudigel *et al*., 2006; Herrera, 2009; Kelly *et al.*, 2011; Staudigel *et al.*, 2014). Predominantly, these alteration textures have a granular appearance, but a fraction of these textures have a distinctive microtubular morphology. Examples of these microtubules are rare and are confined to the upper 100 to 300 m of basement rocks (Staudigel *et al.*, 2008) and are particularly apparent in vitric shards in basalts. Although the diameter and appearance of these tubules may vary from region to region, (McLoughlin, 2007) their morphology has led to the suggestion that they result from fungal excavation (Smits 2006; Etienne and Dupont, 2002; Staudigel *et al.*, 2008). Such alteration textures have been observed in ~3.4 Ga Barberton Greenstone and could potentially be amoungst the eariest morphologial evidence of life (Banergee *et al*., 2006). Impact melt glasses have been observed on Mars (Cannon and Mustard, 2015) and therefore the detection of comprable alteration textures in such formations, may provide evidence of fossilised Martian life (Allen *et al*., 1981).

Such distinctive microtubular features can be observed in the rim of glass shards in the basaltic tuff of the eastern lobe of the Ontong Java Plateau (OJP) (Banerjee and Muehlenbachs, 2003; Miot *et al.*, 2007). The Ontong Java Plateau (OJP) in the southwest Pacific Ocean is the world's largest oceanic igneous province. The OJP covers 1.5 million km^2 and was largely emplaced by a single volcanic event ca. 120 Ma (Tarduno *et al.*, 1991; Mahoney *et al.*, 1993; Fitton *et al.*, 2004). The samples for this study were recovered in the year 2000 during Leg 192 of the Ocean

Drilling Program (ODP) from Hole 1184A located at a water depth of 1661.1 m on the eastern lobe of the OJP (Mahoney, 2001; Ocean_Drilling_Program, 2005). This region consists of tuff rather than the flood basalt that is typical of the main sequence of the OJP (Tarduno *et al.*, 1991; Fitton *et al.*, 2004). Hole 1184A was drilled ahead without coring to 134.4 meters below the seafloor (mbsf) and was rotary cored from 134.4 to 538.8 mbsf with an average recovery of 81.3% (Mahoney et al., 2001). The recovered sequence consists of 201.1 m of calcareous early Miocene nannofossil foraminifera ooze (Unit 1) (Fig. 1) (Ocean Drilling Programme, 2005). This ooze accumulated as the result of the settling of particles to the floor of the open ocean and is formed principally from the calcareous or siliceous shells of either phytoplankton or zooplankton and overlies generally vascular, coarse-grained volcaniclastic rocks, including tuff, lapilli tuff, and lapillistone (Unit 2) separated by an approximately 1-cm-thick ferromanganese crust (Mahoney et al., 2001). Hereafter, the samples OJP_13 OJP_22 and OJP_43 from Unit 2 are collectively described as OJP tuff.

Unit 2 is rich in organic material and consists of at least 6 subunits, 5 of which are delineated by horizons containing the charred and compacted remnants of woody plant material (see Fig 1), these are likely to have arisen as a result of the establishment of terrestrial flora during quiescent periods between each of the volcaniclastic outflow events, implying that its construction from a succession of 6-10 sub-aerial volcaniclastic events (Thordarson, 2004), which was subsequently covered by the calcareous pelagic foraminifera ooze. The microtubules are observed exclusively in the glass shards of core 13R (Banerjee and Muehlenbachs, 2003) (hereafter referred to as OJP_13) in subunit 2A of hole 1184A, where they can be observed ingressing from the perimeter into the centre of every shard within that core sample. The extent and prominence of the

microtubules in OJP_13 has made them ideal specimens to investigate the origins of alteration textures.

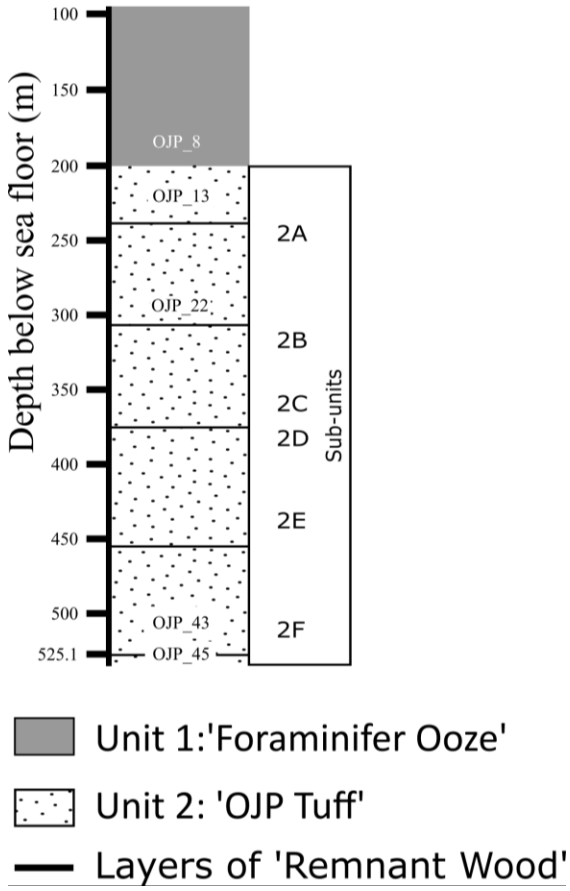

FIG 1. *Diagram of the Ontong java plateau drill hole 1184A site showing acquisition depths of the OJP samples and the stratigraphic layer containing visible wood fragments.* Adapted from Ocean Drilling programme (2001) and Thordarson (2004).

The µm scale distribution of organic material in the OJP_13 has been previously investigated using FTIR microscopy (Preston *et al*, 2011) and by time of flight secondary ion mass spectrometry, thermal hydrolysis and methylation, coupled to gas chromatography/mass spectrometry (THM-GC/MS) and by X-ray photoelectron spectroscopy (XPS) (Sano *et al*, 2016). These investigations demonstrated the heterogeneous distribution of nitrogen containing organic material associated with specific rock textures including rock microfissures as well as the perimeter of the altered glass shards. However, an analysis with THM-GC/MS and XPS of OJP

samples from a range of depths, and other geological samples provides a stratigraphic and geological scale contextual framework, for these earlier studies. Consequently, an OJP_13 sample where microtubular alteration textures were present was compared to tuff samples from the same drill site (Leg 192 Hole 1184A), from core sample 43R (OJP_43) and core sample 22R (OJP_22) where microtubular alteration textures were absent. In addition, and for comparative purposes, a prominent source of organic material in the OJP tuff, namely, the charred woody plant material (OJP_45) was characterised as well as the organic material in the overlaying foraminifera ooze (OJP_8) (Table 1).

To demonstrate that the material detected in the OJP samples was authigenic and not the result of contamination or a procedural artefact, the composition of organic material in basalts from other regions, including the Costa Rica flank (CRB), Atlantic mid-ocean ridge (MAB) and the Whin Sill (WSB) were also characterised. This additional set provided a comparison between the organic composition in the OJP tuff and sub-marine extrusive pillow lava basalts, two of which have been reported to contain glass shards that possess alteration textures (Staudigel *et al*., 2006). The 5 Ma CRB, 80% to 100% of clasts contained granular textures and 0% to 20% contained tubular textures. Whereas the MAB is a 10 Ma sample that possesses glass shards of which 60% to 95% contained granular textures and 5% to 40% contained tubular textures (Furnes *et al.*, 2001). The WSB is a large 295 ± 6 Ma tholeiitic quartz dolerite intrusion in northern England (Fitch and Millar, 1967; Thorpe and Macdonald, 1985) that does not possess glass shards. The CRB, MAB and WSB are collectively described in the article as the ‘basalt samples’.

2.0 Methods

2.1 Sample descriptions and sample preparation for chemical analysis and optical petrography

Table 1 shows the sample geographical locations and depths. All sample cutting was carried out on a Buehler Isomet 1000 and nitrile gloves were worn at all times. Samples were handled with flamed forceps and stored wrapped in Al foil cleaned by sonication in dichloromethane in glass vials. Sections were cut from the internal volumes of parent samples to remove the outer 5-10 mm. The foraminifera ooze (OJP_8) was freeze dried for 48 hours, then 0.5-1.5 g were immobilised by compaction onto an aluminium disk using a manual hydraulic press (Specac Ltd., Orpington, UK).

Identifier	Description	Exp.	Site	Core	Sect.	interval(cm)*	Depth (m.b.s.f.)	Depth into basement (m.)	Glass Shards	Alteration Textures	Location	Ref
OJP_8	Pelagic Ooze	192	1184A	008R	04W	49-51	201.10	-	N/A	N/A	5°0.6653' S 164°13.9771'E	[1,2]
OJP_13	Oceanic tuff	192	1184A	013R	03W	145-148	224.55	23.45	Y	Y	5°0.6653' S 164°13.9771'E	[2,3]
OJP_22	Oceanic tuff	192	1184A	022R	03W	86.5-89	299.99	98.89	Y	N	5°0.6653' S 164°13.9771'E	[1,2, 4]
OJP_43	Oceanic tuff	192	1184A	043R	03W	120-122	495.18	294.08	Y	N	5°0.6653' S 164°13.9771'E	[4]
OJP_45	Wood Fragment	192	1184A	045R	7	48-65	527.61	326.51	N	N	5°0.6653' S 164°13.9771'E	[4]
CRB	Oceanic Basalt	148	896A	011R	01W	111-115	287.10	91.9	Y	Y	1°13.0062'N 83°43.3920'W	[5]
MAB	Oceanic Basalt	46	396B	020R	4W	36-40	291.36	140.86	Y	Y	22°59.1420'N 43°30.9000'W	[6]
WSB	Terrestrial Basalt	-	-	-	-	-	0	-	N	N	N55° 28.427’ 001 35. 577’ W	[7]

Table 1. *The geological samples used for this investigation with acquisition location, depth, the Ocean Drilling Programme data and the sample codes used in this investigation.* [1] Ocean Drilling Programme, (2000); [2] Mahoney *et al*., (2001); [3] Banerjee and Muehlenbachs, (2003); [4] Thordarson, (2004); [5] Dilik, (1998); [6] Furnes *et al*., (2001); [7] Fitch and Millar, (1967)

Optical petrography confirmed the presence or absence of tubule alteration textures in each of the samples. Petrographic thin sections were prepared, immobilised on a microscope slide, ground to a thickness of 30 µm, and covered with a cover-slip (Thin Section Services, Earth Sciences Dept., Durham University). Optical microscopy was conducted using a Leica DM2700M in transmitted light mode. Images were captured using a co-axially mounted Leica DFC450C camera.

2.2 XPS analysis of surface chemistry

XPS is a surface analytical technique capable of obtaining quantitative elemental composition and chemical state measurements in a predefined region with no thermal or solvent extraction and was considered to be complimentary to the bulk THM-GC/MS analysis also carried out in this study. To investigate the composition of residual organic material in the geological samples, XPS was performed, with particular focus on carbon and nitrogen speciation.

To decontaminate surface bound adventitious organic carbon accumulated during sample recovery, storage and processing prior to XPS analysis, gas cluster ion beam (GCIB) etching was conducted for 120 s using nominally 1000 atom Ar clusters at 4 keV over a 1.0 mm x 2.0 mm raster area, within the K-Alpha X-ray photoelectron spectrometer (Thermo Scientific, East Grinstead, UK) instrument, according to Purvis *et al*, (2017). Following decontamination, the samples were immediately analysed without removal from the ultra-high vacuum conditions of the instrument. To obtain a mean value, three positions on each sample were selected for analysis and survey and high-resolution spectra were obtained. The resulting high-resolution spectra were normalised and summed. Synthetic component fitting was conducted using best fit envelopes in the CasaXPS software package (CasaXPS Ltd, Teighmouth, UK), and the chemical states

identified using the analysis in CasaXPS and results from Chastain and King, (2006). Additional chemical state identities were obtained using the NIST database (www.srdata.nist.gov/xps), La surface (www.lasurface.com) and Beamson and Briggs, (1992). The XPS spectra were fitted with peaks that are a mixture of Gaussian and Lorentzian peak shapes, usually described as synthetic components, to create a best-fit (in a least-squared sense)(Cumpson *et al*, 1992). This procedure was performed by the Marquardt linear regression statistical algorithm in the CasaXPS software package (Fairley, 2009). Each of the synthetic peaks that were chosen, was informed by a combination of molecular data obtained by THM-GC/MS and using information based on the NIST and La Surface XPS databases. For future access, the XPS spectral data has been archived in the internationally agreed, ISO14976 format.

The experimental set up in XPS can cause variations in a measured spectral intensity. Thus, the spectral intensity was specified as a relative value, expressed as a fraction of the total surface element composition as an atomic percent (at %) (Watts and Wolstenholme, 2003). This study used the sum of the metal elements Al, Fe, Mg Na and Si occurring at >1 at % in basalt, reference surface concentration that could be used to compare the relative differences in the carbon and nitrogen concentrations between the samples used in this investigation. This baseline was used to measure the differences in carbon concentration resulting from decontamination procedures within WSB by Purvis *et al*., (2017). The column chart (SI, Fig1) shows the consistency of the metal element concentrations of the geological samples used in this investigation.

A 100 × 200 µm elliptical area was selected to provide a mean measurement that would incorporate different geological textures. Three positions were selected for analysis during each

replicate, and three replicates were conducted providing n=9 spectra which were summed using the CasaXPS software.

2.3 THM-GC/MS analysis

Bulk organic analysis was conducted using gas chromatography mass spectrometry (GC/MS) with organic material extracted in-line using pyrolysis in the presence of 10 µl tetramethyl ammonium hydroxide, sometimes called thermal hydrolysis and methylation (THM). Samples were trimmed of surface material then cleaned using a combination of ultra violet light and ozone using a Jelight 144 ultraviolet/ozone (UV/O) cleaner for 20 minutes on each face of the sample, according to (Purvis *et al*, 2017). The trimmed and cleaned samples were then milled in a UV/O decontaminated stainless steel pestle and mortar and passed through a flamed stainless steel 150 µm mesh in a laminar flow cabinet. The THM-GC/MS protocol was adapted from Robertson *et al.* (2008) and was conducted in triplicate. The data was analysed using OpenChrom software (www.openchrom.net) utilising a SNIP baseline deduction, a first derivative peak detection, with the threshold set to medium and the signal:noise set to 2.0. Peak identification was carried out with the NIST05 database. The three compounds with the highest match factor identified by the NIST and were then categorised according to the parent moiety. Where the three the parent moiety NIST assignments disagreed, the compounds were categorised as 'other' in Table 4.

3.0 Results

3.1 Observation of geological textures in petrographic thin sections using Optical Petrography

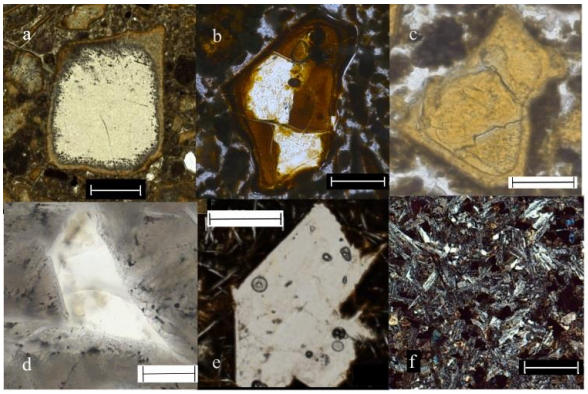

FIG 2 a-f . *Optical petrography of submarine basalts used in this investigation. Figs a-e show a glass shards embedded in a matrix. a. OJP_13, extensive tubular alteration textures are observable in the area around the perimeter of the shard and the orange/brown region is the devitrified rind. Figs: b. OJP_22, c. OJP_43, d. CRB e. MAB, The observed shards in figs b-e do not possess extensive alteration textures. Fig 2f. WSB in which glass shards were absent. Scale bar= 100 µm*

Optical microscopy was able to verify that the microtubular features that were observed in earlier studies (Preston, 2011; Banerjee and Muehlenbachs, 2004) were present only in the OJP_13 samples (Fig 2a) and were absent in all of the other samples (Fig 2b-e). The petrography of the OJP basalt samples (OJP_13, _22 and _43) demonstrated that the glass shards were similar in size to the blocky sub-angular tektite morphology, in agreement with previous reports (Thordarson, 2004). A dark red/brown perimeter was observed in the glass shards of OJP basalt

samples (OJP_13, _22 and _43), which was indicative of weathering, resulting in the devitrification of the glass. The glass shards of the MAB and the CRB were observed as angular shards, demonstrating that the glass shards had formed as a result of rapid quenching in water. The WSB possessed no visually identifiable features, thus no photo micrograph is presented here. These differences permitted a comparison between the OJP samples with tubular textures and those without tubular textures.

3.2 The carbon and nitrogen concentrations measured by XPS.

	Surface concentration (at.%)							
Sample	**OJP_8**	**OJP_13**	**OJP_22**	**OJP_43**	**OJP_45**	**CRB**	**MAB**	**WSB**
C	2.4*	11.8	7.0	11.6	98.2	5.6	2.7	5.2
N	N/D	0.4	0.2	0.4	N/D	N/D	N/D	N/D
N%	N/A	3.4	2.9	3.5	N/A	N/A	N/A	N/A

Table 2: *The surface concentration of carbon and nitrogen. The concentrations are relative to Si, Al, Fe, Mg, Ca, Na (see SI fig 1).*This value excludes the carbon contrition from carbonates that was determined by synthetic peak component fitting.*

The carbon to nitrogen ratio measured using the XPS survey spectra is presented in Table 2. The measurements indicated that the carbon concentration in the control samples (CRB, MAB, and WSB) was approximately half of the carbon concentration in the OJP tuff samples (OJP_13, _22 and_43). Therefore, assuming similar organic matter elemental compositions it would be predicted that the nitrogen concentrations would be in a similar ratio and within the limits of detection for XPS. However, nitrogen was undetected in the CRB, MAB and WSB, implying that nitrogen was absent from these samples. Similarly, nitrogen was not detected in either the foraminifera ooze (OJP_8) or the charred woody fragments (OJP_45) using XPS.

3.3. Characterisation of organic material using XPS

The chemical composition of the carbonaceous material in the geological samples was obtained by taking the mean of the XPS high-resolution spectra for carbon and nitrogen. Synthetic peak component fitting was conducted on the XPS spectra using Beamson and Briggs (1992) and was sufficiently accurate to obtain an indication of the chemical states of the organic material.

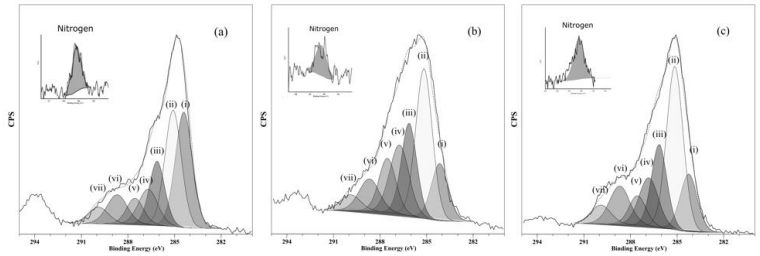

FIG 3 a-c. *High resolution carbon XPS spectra, with high resolution nitrogen spectra inset, for Ontong Java Plateau (OJP) tuffs. (a) OJP_13, (b) OJP_22 and (c) OJP_43. The roman numerals are the key to synthetic components and their assignments (presented in Table 3). The dashed line indicates the best fit envelope for synthetic components. Chemical state assignments for the sythetic components are based on NIST and La Surface databases.*

Fig 3. and Table 3 presents the C1s spectra and data for the OJP tuff samples (OJP_13, _22 and _43) which show that peak components (i) and (ii) which have been assigned to C=C and C-C groups respectively based on their binding energies and these are the most dominant chemical states detected in their C1s spectra. Peak component (iii) is the result of hydroxyl groups also identified by THM-GCMS. The peak component (iv) was a result of a combination of both C-N and C-O chemistry respectively, due to the proximity of the binding energies of these components. Therefore, the peak at 400.5 eV in both the survey spectra and in the high-

resolution N1s spectra confirmed the presence of nitrogen. The 400.5 eV binding energy indicated the chemical state of the nitrogen was N-C (see Fig 3 insets). The C1s component (iv) is divided into (iv a) and (iv b) to distinguish between C-N and C-O chemistry in a single component. Consequently, component (iv a) is assigned to C-N chemistry in the OJP tuff samples. The components (v) and (vi) correspond to carbonyl and carboxyl groups respectively, whereas, component (vii) corresponding to carbonates.

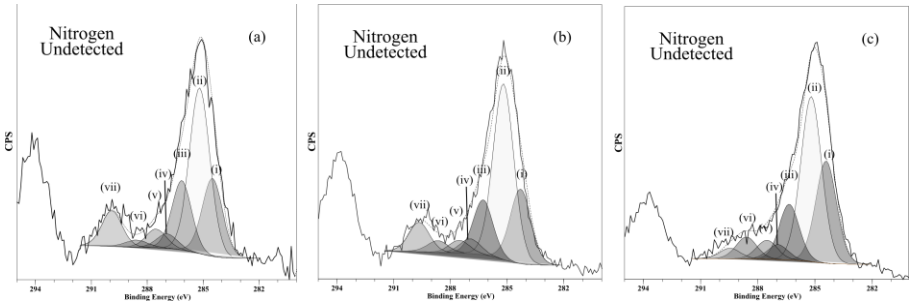

FIG 4 a-c. *High resolution carbon XPS spectra for control samples. (a) Costa Rica pillowlava basalt (CRB), (b) Mid-Atlantic pillow lava basalt (MAB) and (c) Whin Sill basalt (WSB). The Roman numerals are the key to synthetic components and their assignments that are presented in Table 3. The dashed line indicates the best fit envelope for synthetic components. Nitrogen was undetected in these samples.*

The mean high-resolution spectra for carbon and nitrogen were obtained for the basalts from the other regions (CRB, MAB and WSB), (Fig 4 a-c). Carbonaceous material with the chemical states C=C (component i) and C-C (component ii) could be detected as above. However, in contrast to the OJP basalts at all depths, a nitrogen signal could not be detected at 400.5 eV in the high-resolution nitrogen XPS spectra, therefore component (iv) is assigned to C-O chemistry

(Table 3 iv b) (see Fig 3). This difference indicated that the detectable levels of nitrogen were specific to the OJP basalt. In addition to the carbon-carbon chemistry, carbon-oxygen chemistry could be detected in the CRB, MAB and WSB basalts (components iii, v, vi).

The tuff and basalt samples were contrasted with the foraminifera ooze (OJP_8) (Unit 1, in Fig 1), that overlays the OJP tuff and the horizon with wood remnants (horizontal lines, in Fig 1) within the tuff. Fig 5a shows that the high-resolution carbon XPS spectra of OJP_8 is dominated by component (vii). This component was consistent with the presence of carbonates, which were also observed in each of the marine basalts but not in the terrestrial WSB. This observation is consistent with the calcareous nanofossils and planktonic foraminifers that make up Unit 1 (Mahoney et al. 2001). Fig 5b shows the high-resolution carbon XPS spectra from one of the horizons containing fragments of charred woody plant material (OJP_45). The spectra are dominated by component (i) and (ii), whereas components (iii) to (vii) were absent. The data obtained by XPS analysis of the horizon associated with the compacted woody material (Table 4) indicated that nitrogenous organic material was undetected. This result implies that the composition of the organic material in the charred wood fragments in the OJP was different to the organic material in the OJP tuffs.

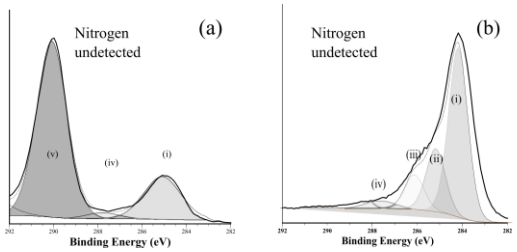

FIG 5 a-b. *High resolution carbon XPS spectra for (a) the foraminifera ooze (OJP_8) and (b) charred plant material (OJP_45). The roman numerals are the key to synthetic components and*

their assignments that are presented in Table 3. The dashed line indicates the best fit envelope for synthetic components. Nitrogen was undetected in these samples.

Component	Binding Energy (eV)	Assignment	Moiety
(i)	284.6	C=C	aromatic
(ii)	285.0	C-C	aliphatic
(iii)	286.4	C-OH	hydroxyl
(iv)	287.0	**C-N***/C-O*	**amide***/furan*
(v)	287.6	C=O	Carbonyl
(vi)	288.6	O-C=O	Carboxyl
(vii)	290	CO_3	*Carbonate*

Table 3: *The key for the XPS synthetic components shown in Figs 3-5 and the chemical states assigned to them. The component binding energy contained a variation of ±0.1 eV in positions to allow the best fit of each synthetic component and were fitted according to Beamson and Briggs* (1992). *Note: The N1s spectra were used to determine whether the component (iv) was assigned to either C-N (bold) or to C-O (italics).*

3.4 Analysis of samples using THM-GC/MS

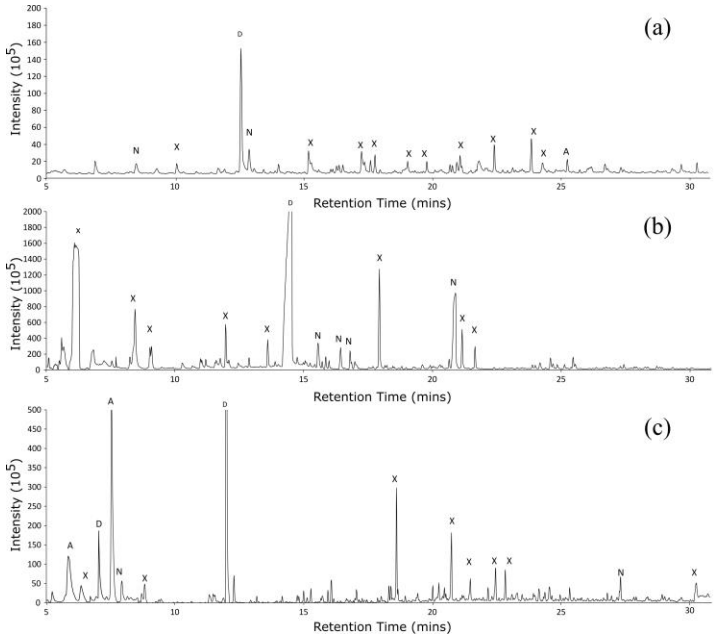

Fig 6 a-c *THM-GC/MS chromatograms of Ontong Java Plateau (OJP) tuffs (a) OJP_13, (b) OJP_22 and (c) OJP_43. The major peaks that could be assigned to a compound with a match factor > 0.7, were annotated (A=Linear/carboxylic acid hydrocarbons; D= decomposed TMAH residues; X= aromatic hydrocarbons; N= nitrogenous heterocycles). The numbers of the compound classes detected in the major and the minor peaks of these samples are tabulated in Table 4.*

Fig 7 a-c THM-GC/MS chromatograms of basalt samples. (a) Costa Rica pillowlava basalt (CRB), (b) Mid-Atlantic pillow lava basalt (MAB) and (c) Whin Sill basalt (WSB). The major peaks that could be assigned to a compound with a NIST library match factor > 0.7, were annotated (*A=Linear/carboxylic acid hydrocarbons; D= decomposed TMAH residues; X= aromatic hydrocarbons; N= nitrogenous heterocycles*). The numbers of the compound classes detected in the major and the minor peaks of these samples are tabulated in Table 4

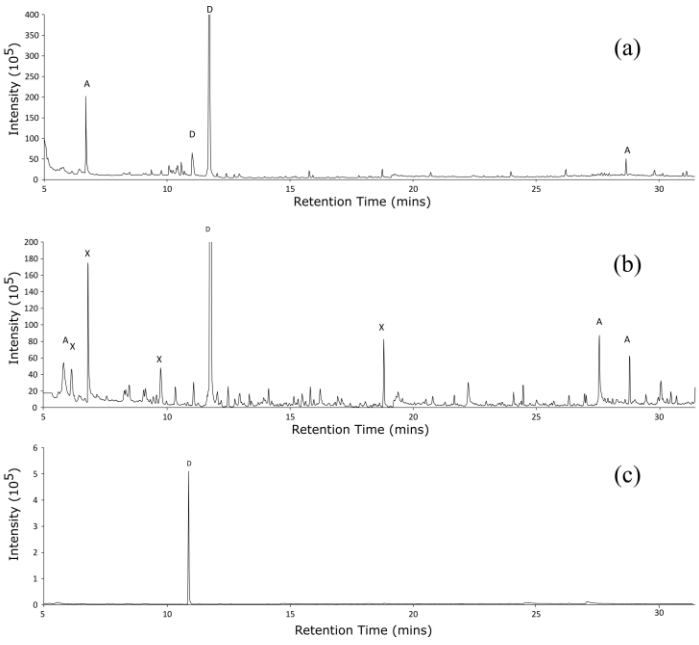

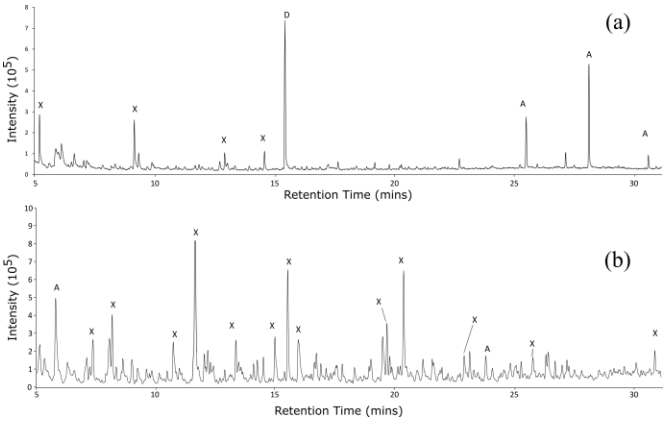

Fig 8 a-b THM-GC/MS chromatograms of (a). OJP_8, and (b) OJP_45. The major peaks that could be assigned to a compound with a NIST library match factor > 0.7, were annotated (*A=Linear/carboxylic acid hydrocarbons; D= decomposed TMAH residues; X= aromatic hydrocarbons; N= nitrogenous heterocycles*). The numbers of the compound classes detected in the major and the minor peaks of these samples are tabulated in Table 4.

The measurements made using XPS demonstrated that the carbon concentration was lower, and that nitrogen was undetected in the CRB, MAB and WSB, whereas the carbon concentration was higher, and nitrogen was present in the OJP tuffs (Table 2). Therefore, it was unsurprising that the total THM-GC/MS derived ion chromatograms for the OJP tuff samples (Fig 6) produced more detectable peaks than those in the basalts, CRB, MAB or WSB (Fig 7). Similarly, THM-GC/MS analysis of OJP_8 resulted in total ion chromatograms with few detectable peaks in comparison to the OJP tuff (Fig 8 a), implying that OJP_8 contained less organic carbon as might be expected for a foraminifera ooze primarily composed of inorganic calcareous carbonates that were undetectable using GC/MS but detectable by XPS (component vii of the C1s spectra in Table 3). In contrast, the buried wood fragments in OJP_45 resulted in a complex range of organic compounds (Fig 8 b).

Precise assignments of peaks to specific organic compounds using THM-GC/MS was not possible, because of their chemical complexity. This complexity also prevented the use of standard compound additions to provide definitive evidence of the presence of specific compounds and resulted in many compounds that were unknown to the NIST database library. This resulted in reverse match factor compound identifications that ranged from 0.7 to 0.9, implying fair to good matches (Stein, 1994; Ausloos *et al.*, 1999; Stein, 2008). To obviate this, a simpler and broader interpretation based on the compound class of the parent moiety of the three closest matches obtained by the NIST library identification was used. This yielded a more confident assignment to general compound classes rather than to a specific compound for each identified peak, and these were presented in Table 4. Aromatic compound assignments (Figs 5-8) are over-represented in the chromatograms in comparison to the full range of compound assignments that could be made in both the major and minor peaks and tabulated in table 4. For comparison, this table also included the similarly derived analysis of the volcanic tephra JSC-1 using THM-GC/MS, which was carried out by Morisson *et al.*, (2017). The major peaks of the chromatograms for the samples where organic material was detected, have been annotated. The key along with attendant table of the ratios of the ten most abundant ions that were used to identify the peaks have been presented in the SI Fig 2 and SI Table.

	OJP_8	**OJP_13**	**OJP_22**	**OJP_43**	**OJP_45**	**CRB**	**MAB**	**WSB**	**JSC-1[1]**
Linear Carboxylic Acids	12	9	4	6	36	5	2	0	32
Linear Hydrocarbons	0	6	0	3	30	5	0	0	13
Alcohols	0	6	0	1	20	1	0	0	11
Amines/Amides	1	4	0	3	0	1	1	1	5
Aromatic hydrocarbons	5	70	28	43	84	3	1	0	87
Cyclic Hydrocarbons	5	9	1	11	56	2	1	0	N/D
Nitrogenous Heterocycles	0	9	7	8	0	0	0	0	30
other	2	3	5	4	12	0	0	0	7
TOTAL	25	116	45	79	238	17	5	1	185

Table 4 *Chemical classes identified in the samples used in this investigation, using THM-GC/MS. [1] For comparison, the compounds identified in the JSC-1 using THM-GC/MS at 600°C* (Morisson *et al*., 2017), *N/D = No data, and includes other heterocycles*.

Table 4 shows that nitrogen substituted heterocyclic (e.g. pyridine) moieties were identified exclusively in the OJP tuff samples (OJP_13, OJP_22 and OJP_43), and these were the only samples where C-N chemistry was observed in the XPS analysis. This suggested that nitrogenous compounds, probably in the form of heterocyclic aromatics, were not specific to the OJP_13 sample, where the alteration textures are observed. In contrast, pyridine moieties were not identified in any samples where nitrogen was absent in the XPS data, specifically the basalts (CRB, MAB and WSB), the pelagic ooze (OJP_8) or the charred wood fragments (OJP_45), implying that while not exclusive to OJP_13, the nitrogenous heterocycles was specific to the OJP tuffs. Additionally, the THM-GC/MS analysis implies that both cyclic and linear hydrocarbons, alcohols and carboxylic acids were identified in the geological samples. This was consistent with the chemical states assigned to the synthetic components of the C1s XPS spectra. (Table 3) and were comparable to the types of organic chemistry detected in the earlier studies of OJP_13 (Sano *et al*, 2016; Preston *et al*., 2011).

4.0 Discussion

Carbonaceous material was detected in each of the geological samples included in this study. This detection included the CRB, MAB and WSB samples in agreement with Furnes *et al* (2001) and Purvis *et al* (2017). However, the quantity, complexity and chemical composition of the organic material in the OJP tuff was very different to the basalt samples and of particular interest is the presence of nitrogen and its association with organic carbon.

Nitrogen was absent in the foraminifera ooze (OJP_8), the wood remnants (OJP_45) and basalts (CRB, MAB, WSB). However, intriguingly and contrary to our expectation it was clear that nitrogen containing compounds were not specific to just OJP_13, where the microtubule alteration textures in the glass shards were exclusively present. Instead, nitrogenous carbon compounds were found to be a general feature of the tuff sequences of the 1184A OJP site irrespective of whether the microtubular features were present or absent. This is of interest because the earlier studies by Preston *et al*. (2011) and Sano *et al*. (2016) both reported the fine scale distribution of the nitrogenous organic matter in OJP_13. The data presented in this current study implies that this nitrogenous organic matter is distributed throughout all of the tuff sequence and, therefore, is not a predictor of tubule formation. This finding highlights the importance of conducting analysis at a range of spatial scales to provide a complete organic geochemical context in the search for fossilised life on Earth and eventually on Mars.

With respect to the origin of this nitrogen rich organic material in the OJP tuff, the much lower concentrations of organic material and indeed absence of nitrogen in the overlying foraminifera ooze suggests that it was not simply a result of diffusion from the overlying unit 1 into unit 2. Therefore, an additional possibility to explain raised levels of organics in the tuff is the diffusion of organic material from the horizons of plant material that were buried during the volcaniclastic outflows, to other parts of the unit. The tuff of Unit 2 is vascular with porosities measured at ~30-35% (Thordarson, 2004; Ocean Drilling Programme, 2005) and the partial anoxic combustion of plant material (charring) results primarily in aromatic compounds (Wiedemeier *et al.*, 2015), compounds that were observed in both the OJP_45 and in the OJP tuff samples, despite the reported absence of woody materials in these intervening tuff horizons and now

verified by our optical petrography. Lignin phenols were, however, absent from the THM products probably due to thermally driven degradation processes (Vane *et al*., 1999).

The absence of nitrogenous compounds in the Charred wood fragments (OJP_45) was surprising, since nitrogen is often detected in low concentrations in char, depending on feedstock and the formation processes. However, solid char N can be converted to gaseous NO at high temperatures (Jones *et al*., 2004). Although the temperature of the tuff during deposition cannot be known, this observation lead us to speculate that it was sufficiently high enough to permit the conversion process and the resultant loss to take place. This non-detection of nitrogen indicated that it is different to the organic material in the other OJP tuff sections, which argues against the possibility that the organic material in the OJP tuff originated from the charred wood horizons. Interestingly, this wood derived organic material could have potentially served as a substrate for organotrophic endolithic organisms present in the tuff resulting in the accumulation of biomass from any endolithic organisms.

Nitrogen is present in all organisms, however, some taxa use amine-containing chitin as their primary structural biopolymer, including arthropods, insects, sponges and fungi (Bowman and Free, 2006), and the presence of chitin could explain the elevated nitrogen concentrations. We note that the pyridine based compounds detected in the OJP_13, OJP_22 and OJP_43 using THM-GC/MS resembled some of the pyridine based compounds detected in arthropod cuticle (Stankiewicz *et al*., 1996) and artificially matured chitin (Gupta *et al*, 2006) with pyrolysis GC/MS. Additionally, our XPS and THM-GC/MS data were comparable to the carbon nitrogen chemistry detected in fossilised arthropods with X-ray absorption near edge structure (XANES) (Cody *et al*, 2011) and is in agreement with the detection of pyridines and pyrimidines in kerogen using XPS analysis (Boudou *et al*., 2008), which demonstrated that nitrogen is

incorporated into polyaromatic compounds during diagenesis and catagenesis. In general, after early diagenesis, 1-2% of carbonaceous nitrogen is preserved (Schimmelmann and Lis, 2010). This is contrasted with the 2.5 % to 3.4 % carbonaceous nitrogen observed in the OJP tuffs. The tubular morphology seen in OJP_13 and elsewhere have been suggested to be the result of fungal excavation (Smits, 2006; Staudigel *et al.*, 2008) and there is evidence of a fungal community in the submarine crust (Bengtson *et al.*, 2014; Ivarsson *et al.*, 2015; Ivarsson *et al.*, 2016) and thus fungi may have been present in the OJP tuff. However, our evidence indicates that such putative fungal activity does not necessarily result in rock alteration textures. Therefore, it is not inconceivable that the trigger for excavation might require unknown local factors (McLoughlin *et al.*, 2010; Cockell and Herrera., 2008). These factors could include differences in nutrient concentrations, or the proximity to the surface of the OJP_13 sample, prior to the subsequent burial by the pelagic ooze sediment (Fig 1, Unit 1).

5.0 Conclusion

The study by Preston *et al*., (2011) and Sano *et al.*, (2016) demonstrated that nitrogenous organic material was heterogeneously distributed at the µm scale in micro-fissures and in the weathered perimeter of glass shards in the OJP_13. Across the samples in our study, only the OJP tuffs showed elevated concentrations of nitrogenous organic material. In contrast, nitrogenous organic material was not detected in either the overlaying sediment (OJP_8) or the charred woody material (OJP_45) indicating that neither of these were the source of the nitrogen. Similarly, nitrogenous material was not detected in the basalt samples from other regions. This result implies that the composition of the organic material in the OJP tuff is different to the other geological samples investigated here and that nitrogen concentration is higher. This difference could potentially be the result of the presence the fungi that are found in the submarine crust,

although further investigations to verify this are required. However, the evidence from our stratigraphic study indicates that the composition of the organic material is not corelated to the presence or absence of microtubular alteration textures in the glass shards of the OJP tuffs.

443

444 **References**

Allen, C.C., Gooding, J.L., Jercinovic, M. and Keil, K., (1981). Altered basaltic glass: A terrestrial analog to the soil of Mars. *Icarus*, *45*(2), pp.347-369.

Alt, J.C. and Mata, P. (2000) 'On the role of microbes in the alteration of submarine basaltic glass: a TEM study', *Earth and Planetary Science Letters*, 181(3), pp. 301-313.

Ausloos, P., Clifton, C.L., Lias, S.G., Mikaya, A.I., Stein, S.E., Tchekhovskoi, D.V., Sparkman, O.D., Zaikin, V. and Zhu, D. (1999) 'The critical evaluation of a comprehensive mass spectral library', *Journal of the American Society for Mass Spectrometry*, 10(4), pp. 287-299.

Banerjee, N.R. and Muehlenbachs, K. (2003) 'Tuff life: Bioalteration in volcaniclastic rocks from the Ontong Java Plateau', *Geochemistry Geophysics Geosystems*, 4.

Banerjee, N.R., Furnes, H., Muehlenbachs, K., Staudigel, H. and de Wit, M. (2006) 'Preservation of ~3.4–3.5 Ga microbial biomarkers in pillow lavas and hyaloclastites from the Barberton Greenstone Belt, South Africa', *Earth and Planetary Science Letters*, 241(3-4), pp. 707-722.

Beamson, G., & Briggs, D. (1992) *High resolution XPS of organic polymers: the Scienta ESCA300 database* Chichester: Wiley.

Bengtson, S., Ivarsson, M., Astolfo, A., Belivanova, V., Broman, C., Marone, F. and Stampanoni, M. (2014) 'Deep-biosphere consortium of fungi and prokaryotes in Eocene subseafloor basalts', *Geobiology*, 12(6), pp. 489-496.

Boudou, J.P., Schimmelmann, A., Ader, M., Mastalerz, M., Sebilo, M. and Gengembre, L., (2008). Organic nitrogen chemistry during low-grade metamorphism. *Geochimica et Cosmochimica Acta*, *72*(4), pp.1199-1221

Bowman, S.M. and Free, S.J. (2006) 'The structure and synthesis of the fungal cell wall', *Bioessays*, 28(8), pp. 799-808.

Cockell, C.S. and Herrera, A., (2008). Why are some microorganisms boring?. *Trends in microbiology*, *16*(3), pp.101-106.

Cannon, K.M. and Mustard, J.F., (2015). Preserved glass-rich impactites on Mars. *Geology*, *43*(7), pp.635-638

Cody, G.D., Gupta, N.S., Briggs, D.E.G., Kilcoyne, A.L.D., Summons, R.E., Kenig, F., Plotnick, R.E. and Scott, A.C. (2011) 'Molecular signature of chitin-protein complex in Paleozoic arthropods', *Geology*, 39(3), pp. 255-258.

Chastain, J., & King, R. C. (Eds.). (1995) *Handbook of X-ray photoelectron spectroscopy: a reference book of standard spectra for identification and interpretation of XPS data*. Eden Prairie, MN: Physical Electronics.

PJ Cumpson, MP Seah, Random uncertainties in AES and XPS: I: Uncertainties in peak energies, intensities and areas derived from peak synthesis Surface and Interface analysis 18 (1992) 345-360

Dilik, Y. (1998) *Structure and Techtonics of Intermeiate-Spread Oceanic Crust Drilled at DSDP/ODP holes 504B and 896A, Costa Rica Rift*. London: Geological Society of London.

Fairley, N. (2009) CasaXPS Manual 2.3. 15: Introduction to XPS and AES. Available at: www.casaxps.com/ebooks/OrangeBookRev1.3ebook.pdf

Fisk, M.R., Giovannoni, S.J. and Thorseth, I.H. (1998) 'Alteration of oceanic volcanic glass: Textural evidence of microbial activity', *Science*, 281(5379), pp. 978-980.

Fitch, F.J.and.Millar., J. A. (1967) 'The age of the Whin Sill', *Geological Journal*, 5(2), pp. 233–250.

Fitton, J.G., Godard, M., Mahoney, J.J. and Herzberg, C. (2004) 'Origin of the Ontong Java Plateau', *Geochimica Et Cosmochimica Acta*, 68(11), pp. A581-A581.

Furnes, H., Muehlenbachs, K., Torsvik, T., Thorseth, I.H. and Tumyr, O. (2001) 'Microbial fractionation of carbon isotopes in altered basaltic glass from the Atlantic Ocean, Lau Basin and Costa Rica Rift', *Chemical Geology*, 173(4), pp. 313-330.

Gupta, N.S., Michels, R., Briggs, D.E.G., Evershed, R.P. and Pancost, R.D. (2006) 'The organic preservation of fossil arthropods: an experimental study', *Proceedings of the Royal Society B-Biological Sciences*, 273(1602), pp. 2777-2783.

Herrera, A., Cockell, C. S., Self, S., Blaxter, M., Reitner, J., Thorsteinsson, T.,& Tindle, A. (2009) 'A cryptoendolithic community in volcanic glass', *Astrobiology*, 9(4), pp. 369-381.

Ivarsson, M., Bengtson, S., Skogby, H., Lazor, P., Broman, C., Belivanova, V. and Marone, F. (2015) 'A Fungal-Prokaryotic Consortium at the Basalt-Zeolite Interface in Subseafloor Igneous Crust', *Plos One*, 10(10).

Ivarsson, M., Bengtson, S., & Neubeck, A. (2016). The igneous oceanic crust–Earth's largest fungal habitat?. *Fungal Ecology*, *20*, 249-255.

Jones JM, Pourkashanian M, Williams A, Rowlands L, Zhu Q, Thomas KM. (2004), Conversion of char nitrogen to NO during combustion. Journal of the Energy Institute 77(513), 82-89.

Kelly, L.C., Cockell, C.S., Herrera-Belaroussi, A., Piceno, Y., Andersen, G., DeSantis, T., Brodie, E., Thorsteinsson, T., Marteinsson, V., Poly, F. and LeRoux, X. (2011) 'Bacterial diversity of terrestrial crystalline volcanic rocks, Iceland', *Microb Ecol*, 62(1), pp. 69-79.

Mahoney, J.J., Storey, M., Duncan, R. A., Spencer, K. J., & Pringle, M. (1993) 'Geochemistry and age of the Ontong Java Plateau.', *The Mesozoic Pacific: Geology, Tectonics, and Volcanism, Geophys. Monogr. Ser*, 77, pp. 233-261.

Mahoney, J.J., Fitton, J.G. and Wallace, J., (2001) 'Leg 192 Summary', *Shipboard Scientific Party, In Proceedings of the Ocean Drilling Program, Initial Reports* 192,, pp. 1-75.

McBride, N. and Gilmour, I. (2004) An Introduction to the Solar System. Cambridge University Press.

McLoughlin, N., Brasier, M.D., Wacey, D., Green, O.R. and Perry, R.S. (2007) 'On biogenicity criteria for endolithic microborings on early Earth and beyond', *Astrobiology*, 7(1), pp. 10-26.

McLoughlin, N., Staudigel, H., Furnes, H., Eickmann, B. and Ivarsson, M., (2010). Mechanisms of microtunneling in rock substrates: distinguishing endolithic biosignatures from abiotic microtunnels. *Geobiology*, *8*(4), pp.245-255.

Miot, J., Benzerara, K., Banerjee, N.R., Menguy, N., Tyliszczak, T., Brown, G.E. and Guyot, F. (2007) 'Study at the nanoscale of the alteration of submarine basaltic glass from the Ontong Java Plateau', *Geochimica Et Cosmochimica Acta*, 71(15), pp. A671-A671.

Morisson, M., A and Szopa, C and Raulin, F and Stambouli, M (2017) 'TMAH Thermochemolysis of a Martian Regolith Simulant: Optimization of an Analytical Method for the Detection of Trace Organic Matter by the MOMA-Pyr-GC-MS Experiment Onboard the ExoMars-2020 Rover', *Lunar and Planetary Science XLVIII*. Heterocycles. Available at: https://www.hou.usra.edu/meetings/lpsc2017/pdf/1079.pdf.

Ocean Drilling Program (2005) *Archive of Core and Site/Hole Data and Photographs from the Ocean Drilling Program (ODP)* (Accessed: 15 September).

Preston, L.J., Izawa, M.R. and Banerjee, N.R. (2011) 'Infrared spectroscopic characterization of organic matter associated with microbial bioalteration textures in basaltic glass', *Astrobiology*, 11(7), pp. 585-99.

Purvis, G., Gray, N., Sano, N., Barlow, A., Cockell, C., Abbott, G.D., van der Land, C., Cumpson, P., (2017) 'Decontamination of geological samples by gas cluster ion beam etching or ultra violet/ozone', *Chemical Geology*, In Press. DOI 10.1016/j.chemgeo.2017.06.016

Robertson S.A., Mason S.L., Hack E, Abbott G.D., 2008. A comparison of lignin oxidation, enzymatic activity and fungal growth during white-rot decay of wheat straw. Organic Geochemistry 39, 945–951.

Sano, N., Purvis, G.W.H., Barlow, A.J., Abbott, G.D., Gray, N.N.D. and Cumpson, P.J. (2016) 'Gas cluster ion beam for the characterization of organic materials in submarine basalts as Mars analogs', *Journal of Vacuum Science & Technology A*, 34(4).Schimmelmann, A., Wintsch, R.P., Lewan, M.D. and DeNiro, M.J. (1998) 'Chitin: 'Forgotten' source of nitrogen - From modern chitin to thermally mature kerogen: Lessons from nitrogen isotope ratios', *Nitrogen-Containing Macromolecules in the Bio- and Geosphere*, 707, pp. 226-242.

Schimmelmann, A., Wintsch, R.P., Lewan, M.D. and DeNiro, M.J., (1998). Chitin:'Forgotten'Source of Nitrogen: From Modern Chitin to Thermally Mature Kerogen: Lessons from Nitrogen Isotope Ratios.

Schimmelmann, A. and Lis, G.P. (2010) 'Nitrogen isotopic exchange during maturation of organic matter', *Organic Geochemistry*, 41(1), pp. 63-70.

Smits, M.M. (2006) ' Mineral Tunnelling by Fungi.', in Gadd, G.M.E. (ed.) *Fungi in Biogeochemical Cycles. .* Cambridge: Cambridge University Press, pp. 681–717.

Stankiewicz, B.A., Briggs, D.E.G., Evershed, R.P., Duncan, I.J., vanBergen, P.F. and Hof, C.H.J. (1996) 'In research of chitin: Pyrolysis-GC/MS studies of modern, decayed and fossil arthropod cuticles.', *Abstracts of Papers of the American Chemical Society*, 212, pp. 11-Geoc.

Staudigel, H., Banergee,N.,Dilek,Y.,& Muehlenbachs,K. (2006) 'Microbes and volcanoes: A tale from the oceans, ophiolites, and greenstone belts', *GSA Today*, 16(10).

Staudigel, H., Furnes, H., McLoughlin, N., Banerjee, N.R., Connell, L.B. and Templeton, A. (2008) '3.5 billion years of glass bioalteration: Volcanic rocks as a basis for microbial life?', *Earth-Science Reviews*, 89(3-4), pp. 156-176.

Staudigel, H., Furnes, H. and Smits, M. (2014) 'Deep Biosphere Record of In Situ Oceanic Lithosphere and Ophiolites', *Elements*, 10(2), pp. 121-126.

Stein, S.E. (1994) 'Estimating Probabilities of Correct Identification from Results of Mass-Spectral Library Searches', *Journal of the American Society for Mass Spectrometry*, 5(4), pp. 316-323.

Stein, S.E., (2008). NIST standard reference database 1A. *National Institute of Standards and Technology, Gaithersburg*.

Tarduno, J.A., Sliter, W.V., Kroenke, L., Leckie, M., Mayer, H., Mahoney, J.J., Musgrave, R., Storey, M. and Winterer, E.L. (1991) 'Rapid Formation of Ontong Java Plateau by Aptian Mantle Plume Volcanism', *Science*, 254(5030), pp. 399-403.

Thordarson, T. (2004) 'Accretionary-lapilli-bearing pyroclastic rocks at ODP Leg 192 Site 1184: A record of subaerial phreatomagmatic eruptions on the Ontong Java Plateau', *Geological Society, London, Special Publications*, 229(1), pp. 275-306.

Thorpe, R.S. and Macdonald, R. (1985) 'Geochemical Evidence for the Emplacement of the Whin Sill Complex of Northern England', *Geological Magazine*, 122(4), pp. 389-396.

Vane, C.H. and Abbott, G.D., 1999. Proxies for land plant biomass: Closed system pyrolysis of some methoxyphenols. Organic Geochemistry 30, 1535–1541

Watts, J.F. and Wolstenholme, J. (2003) *An Introduction to surface analysis by XPS and AES*. Wiley Chichester.

Wiedemeier, D.B., Abiven, S., Hockaday, W.C., Keiluweit, M., Kleber, M., Masiello, C.A., McBeath, A.V., Nico, P.S., Pyle, L.A., Schneider, M.P.W., Smernik, R.J., Wiesenberg, G.L.B. and Schmidt, M.W.I. (2015) 'Aromaticity and degree of aromatic condensation of char', *Organic Geochemistry*, 78, pp. 135-143.

Acknowledgments

The Author is deeply grateful for the grant generously provided by The Leverhulme Trade Charities Trust without which this project would not be possible. Many thanks also to the IODP Gulf of Mexico repository in Texas for the supply of Geological samples, and all the team at NEXUS, Newcastle University. Thanks to Paul Donohoe for operating the pyrolysis-GCMS.

Funding: Leverhulme Trade Charities Trust

Supplementary Figures

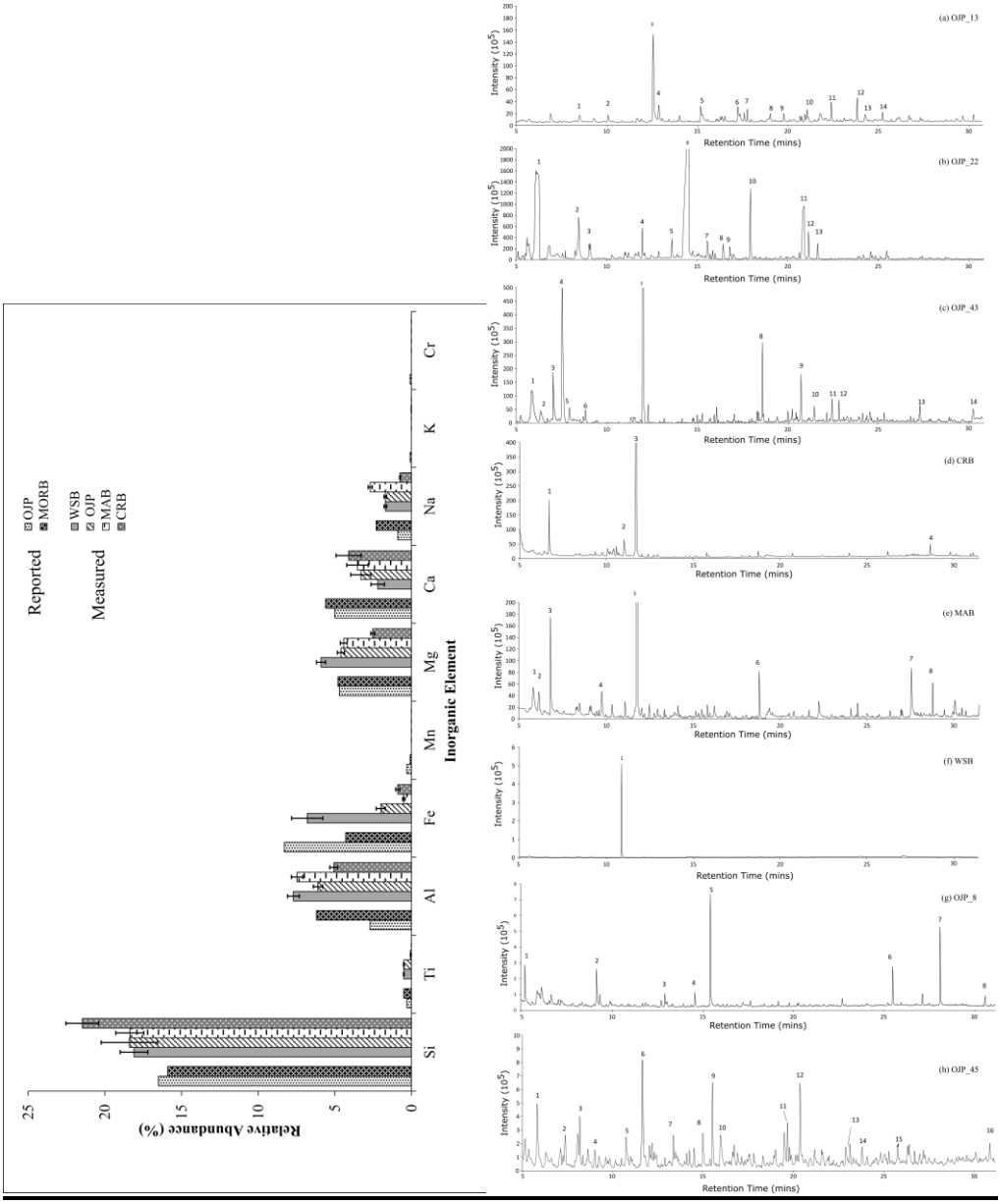
Reported
OJP
MORB
Measured
WSB
OJP
MAB
CRB
Relative Abundance (%)
Inorganic Element
Si
Ti
Al
Fe
Mn
Mg
Ca
Na
K
Cr
(a) OJP_13
(b) OJP_22
(c) OJP_43
(d) CRB
(e) MAB
(f) WSB
(g) OJP_8
(h) OJP_45
Intensity (10^5)
Retention Time (mins)

452

Supplementary peak assignments

(a) OJP_13

Peak	**m/z**	abund	**m/z**	abund	**m/z**	abund	**m/z**	abund	**m/z**	abund	peak assignment
1	**57**	4	**58**	100	**59**	4	**61**	5	**73**	1	**Butylamine**
2	**78**	100	**92**	13	**93**	17	**105**	23	**106**	51	**3-Ethylpyridine**
3	**58**	36	**59**	25	**89**	24	**91**	100	**106**	44	Ethylbenzene
4	**65**	69	**77**	21	**78**	61	**79**	18	**108**	100	Methoxybenzene
5	**77**	13	**86**	12	**105**	100	**119**	12	**120**	47	Isopropylbenzene
6	**57**	32	**91**	23	**105**	100	**119**	62	**120**	54	**Butylpyridine**
7	**77**	41	**79**	40	**90**	22	**107**	89	**108**	100	4-Methylphenol
8	**91**	100	**92**	17	**107**	15	**119**	29	**120**	71	Meta Tolualdehyde
9	**91**	42	**115**	58	**117**	100	**131**	18	**132**	96	1-Propenyl-Toluene
10	**77**	40	**91**	34	**107**	98	**121**	42	**122**	100	2,3-Dimethylphenol
11	**91**	16	**119**	100	**120**	10	**133**	9	**134**	47	1-Isopropyl-4-Methylbenzene
12	**77**	13	**91**	22	**117**	11	**119**	100	**134**	47	1-Isopropyl-4-Methylbenzene
13	**91**	19	**105**	14	**119**	19	**135**	100	**150**	26	Ortho-Methoxyacetophenone
14	**91**	12	**115**	10	**133**	100	**134**	12	**148**	30	Pentamethylbenzene

(b) OJP_22

Peak #	**m/z**	abund	**m/z**	abund	**m/z**	abund	**m/z**	abund	**m/z**	abund	peak assignment
1	**92**	28	**91**	46	**70**	66	**69**	100	**53**	5	phenylacetic acid

2	**106**	54	**105**	24	**93**	38	**92**	20	**91**	100	1,3-dimethyl benzene
3	**104**	100	**103**	47	**78**	33	**77**	18	**51**	11	styrene
4	**120**	50	**119**	14	**118**	17	**117**	21	**105**	100	1,3,5-trimethyl-benzene,
5	**117**	9	**116**	99	**115**	100	**108**	13	**89**	10	1-ethynyl-4-methyl-benzene,
6	**109**	67	**108**	100	**83**	53	**82**	28	**67**	36	TMAH
7	**123**	11	**109**	8	**108**	100	**97**	6	**67**	9	**3-acetyl-1-methylpyrrole**
8	**123**	10	**109**	6	**108**	100	**95**	3	**67**	9	**2,6-dimethyl-pyrazine,**
9	**130**	100	**129**	80	**128**	39	**127**	18	**115**	85	benzene,
10	**129**	11	**128**	100	**127**	12	**126**	7	**102**	7	naphthalene
11	**152**	2	**126**	9	**84**	6	**83**	100	**67**	2	**1-methyl-1h-1,2,4-triazole**
12	**143**	11	**142**	100	**141**	84	**139**	10	**115**	24	1-methyl-naphthalene
13	**143**	12	**142**	100	**141**	88	**139**	11	**115**	26	1-methyl-naphthalene

(c)OJP_43

Peak #	**m/z**	abund	**m/z**	abund	**m/z**	abund	**m/z**	abund	**m/z**	abund	peak assignment
1	**94**	100	**84**	12	**83**	18	**79**	48	**61**	10	dimethyl disulfide,
2	**93**	5	**92**	60	**91**	100	**65**	9	**63**	6	2-propenylidene cyclobutene,
3	**74**	4	**73**	100	**72**	7	**58**	4	**56**	2	n,n-dimethyl-formamide,
4	**61**	5	**59**	4	**58**	100	**57**	4	**56**	2	acetone
5	**95**	62	**94**	100	**93**	8	**78**	6	**53**	9	**2,5-dimethyl-1h-pyrrole,**
6	**106**	35	**105**	26	**103**	7	**93**	4	**91**	100	xylene
7	**129**	31	**128**	100	**86**	96	**85**	11	**57**	31	TMAH
8	**138**	5	**137**	57	**136**	100	**134**	3	**122**	38	phenol
9	**148**	45	**147**	9	**134**	9	**133**	100	**115**	7	pentamethyl-benzene,
10	**159**	14	**158**	63	**143**	100	**141**	24	**115**	19	1,2,3-trimethylindene
11	**165**	14	**162**	28	**148**	13	**147**	100	**136**	57	3,3-dimethyl-isobenzofuranone
12	**162**	35	**148**	13	**147**	100	**133**	12	**115**	4	1,2-diethyl-3,4-dimethyl-benzene,
13	**163**	7	**162**	50	**161**	6	**148**	12	**147**	100	6-methoxy-3-methylbenzofuran
14	**170**	17	**159**	80	**158**	100	**155**	17	**144**	44	2,3,5-trimethyl-1h-indole,

(d) CRB

Peak #	**m/z**	abund	**m/z**	abund	**m/z**	abund	**m/z**	abund	**m/z**	abund	peak assignment
1	**56.05**	2	**58.05**	8	**72.05**	8	**73.05**	100	**74.05**	51	Dimethyl-Formamide
2	**57.05**	45	**85.05**	14	**86.05**	100	**128.05**	89	**129.15**	68	TMAH
3	**57.05**	42	**85.05**	13	**86.05**	100	**128.15**	96	**129.15**	74	TMAH
4	**55.05**	52	**56.05**	16	**57.05**	100	**71.05**	69	**85.05**	47	Hexadecane

(e)MAB

Peak #	**m/z**	abund	**m/z**	abund	**m/z**	abund	**m/z**	abund	**m/z**	abund	peak assignment
1	**84**	56	**83**	100	**79**	45	**58**	96	**52**	15	Acetone
2	**92**	60	**91**	100	**83**	53	**65**	11	**58**	29	2-propenylidene-Cyclobutene
3	**74**	50	**73**	100	**72**	8	**58**	9	**56**	2	N,N-dimethyl-Formamide,
4	**108**	100	**79**	17	**78**	62	**77**	32	**65**	65	methoxy-benzene
5	**129**	73	**128**	93	**86**	100	**85**	13	**57**	42	TMAH
6	**141**	11	**87**	46	**74**	100	**59**	61	**55**	21	Nonanoic acid
7	**152**	97	**111**	59	**83**	87	**74**	80	**55**	100	dimethyl ester nonanedioic acid
8	**85**	44	**71**	66	**57**	100	**56**	16	**55**	52	Hexadecane

(f) WSB: No Major peaks were detected, no minor peaks were identified with a reverse match factor of >0.7

(g) OJP_8

Peak #	**m/z**	abund	**m/z**	abund	**m/z**	abund	**m/z**	abund	**m/z**	abund	peak assignment
1	**104**	100	**103**	47	**78**	36	**77**	17	**51**	19	styrene
2	**112**	62	**69**	41	**68**	94	**56**	54	**55**	100	2 methyl cyclohexanone
3	**120**	33	**105**	100	**78**	9	**77**	79	**51**	24	1-phenylethanone
4	**136**	38	**105**	100	**77**	56	**51**	19	**50**	8	methyl ester benzoic acid
5	**138**	92	**129**	100	**97**	73	**74**	84	**69**	83	dimethyl ester octanedioic acid,
6	**194**	22	**164**	11	**163**	100	**135**	21	**103**	12	1,4-dimethyl ester benzenedicarboxylic a
7	**185**	56	**152**	100	**83**	60	**74**	69	**55**	83	dimethyl ester nonanedioic acid,
8	**199**	100	**125**	94	**98**	64	**74**	94	**55**	63	10-chloro-10-oxo-methyl ester decanoic

(h) OJP_45

Peak #	**m/z**	abund.	**m/z**	abund.	**m/z**	abund.	**m/z**	abund.	**m/z**	abund.	Peak assignment
1	**105.1**	1	**61.1**	5	**59.1**	5	**58.1**	100	**56.1**	2	acetone
2	**106.1**	54	**105.1**	24	**91.1**	100	**81.1**	17	**77.1**	15	Xylene
3	**106.1**	50	**98.1**	41	**91.1**	100	**69.1**	26	**55.1**	68	Xylene
4	**85.1**	47	**71.1**	33	**57.1**	100	**56.1**	31	**55.1**	34	Nonane
5	**108.1**	100	**79.1**	19	**78.1**	57	**77.1**	20	**65.1**	54	methoxybenzene
6	**106.1**	100	**105.1**	98	**77.1**	89	**51.1**	31	**50.1**	19	Benzalderhyde
7	**95.1**	8	**94.1**	100	**66.1**	30	**65.1**	22	**55.1**	7	Phenol
8	**120.1**	49	**105.1**	100	**95.1**	31	**79.1**	19	**67.1**	23	trimethybenzene
9	**122.1**	100	**121.1**	46	**107.1**	30	**91.1**	34	**77.1**	41	Methoxybenzene
10	**108.1**	100	**107.1**	89	**105.1**	12	**91.1**	12	**90.1**	23	3 methyl phenol

11	**120.1**	39	**106.1**	9	**105.1**	100	**77.1**	69	**51.1**	19	acetophenone
12	**108.1**	84	**107.1**	100	**79.1**	21	**77.1**	25	**51.1**	9	4-methyl Phenol
13	**134.1**	100	**119.1**	58	**91.1**	48	**65.1**	20	**135.1**	11	Benzene, 1-ethenyl-4-methoxy-
14	**122.1**	33	**108.1**	8	**107.1**	100	**91.1**	6	**77.1**	16	4-ethylphenol
15	**129.1**	14	**128.1**	100	**127.1**	14	**121.1**	8	**102.1**	7	Naphthalene
16	**85.1**	50	**71.1**	71	**57.1**	100	**56.1**	16	**55.1**	24	Tetradecane

SI Table 1: *The peak assignments (peak#) obtained from the NIST05 library with the corresponding abundances (abund) and mass/charge ratios of the 5 most abundant ions of foraminifer ooze (OJP_8); Ontong Java Plateau tuff (OJP_22; OJP_13, OJP_43); Charred wood fragments (OJP_45); Mid-Atlantic ridge pillow lava basalt (MAB); Costa Rica Flank pillow lava basalt (CRB) and Whin Sill basalt (WSB*).

Qualifications and Statement of Financial Interest

Graham Purvis	Master of Science	**No competing financial interests exist**
Neil Grey	Doctor	
Naoko Sano	Doctor	
Charles Cockell	Professor	
Anders Barlow	Doctor	
Elisa Lopez-Capel	Doctor	
Peter Cumpson	Professor	